Hindawi
Advances in Meteorology
Volume 2020, Article ID 9290837, 14 pages
https://doi.org/10.1155/2020/9290837

Research Article

A Survey on the Relationship between Ocean Subsurface Temperature and Tropical Cyclone over the Western North Pacific

Difu Sun,[1,2] Junqiang Song,[1,2] Kaijun Ren,[1,2] Xiaoyong Li,[1,2] and Guangjie Wang[3]

[1]*College of Meteorology and Oceanography, National University of Defense Technology, Changsha 410073, China*
[2]*College of Computer Science and Technology, National University of Defense Technology, Changsha 410073, China*
[3]*Unit 61741 of People's Liberation Army, Beijing 100080, China*

Correspondence should be addressed to Xiaoyong Li; sayingxmu@nudt.edu.cn

Received 3 February 2020; Accepted 22 July 2020; Published 20 August 2020

Academic Editor: Harry D. Kambezidis

The relationship between ocean subsurface temperature and tropical cyclone (TC) over the western North Pacific (WNP) is studied based on the TC best-track data and global reanalysis data during the period of 1948–2012. Here the TC frequency (TCF), lifespan, and genesis position of TCs are analysed. A distinctive negative correlation between subsurface water temperature and TCF is observed, especially the TCF in the southeastern quadrant of the WNP (0–15°N, 150–180°E). According to the detrended subsurface temperature anomalies of the 125 m depth layer in the main TC genesis area (0–30°N, 100–180°E), we selected the subsurface cold and warm years. During the subsurface cold years, TCs tend to have a longer mean lifespan and a more southeastern genesis position than the subsurface warm years in general. To further investigate the causes of this characteristic, the TC genesis potential indexes (GPI) are used to analyse the contributions of environmental factors to TC activities. The results indicate that the negative correlation between subsurface water temperature and TCF is mainly caused by the variation of TCF in the southeastern quadrant of the WNP, where the oceanic and atmospheric environments are related to ocean subsurface conditions. Specifically, compared with the subsurface warm years, there are larger relative vorticity, higher relative humidity, smaller vertical wind shear, weaker net longwave radiation, and higher ocean mixed layer temperature in the southeastern quadrant during cold years, which are all favorable for genesis and development of TC.

1. Introduction

Tropical cyclone (TC) is one of the most hazardous natural phenomena on Earth, which causes huge damage to human life and property for billions of people [1, 2]. As one of the most active regions for TCs, the western North Pacific (WNP) basin experiences about 1/3 of the global TCs every year, which reach on average about 26 TCs annually [3]. The enormous quantity of TC activities over the WNP mainly results from a favorable large-scale environment including atmospheric circulation systems [4–6] and interaction between ocean and atmosphere [7, 8].

As a crucial factor in the air-sea interaction, sea-surface temperature (SST) has attracted widespread attention in the research of TC [9–12]. A relatively high SST surrounding is critical for the genesis of TC, and there is an established fact that SST >26°C is a requirement for TC formation [13–15], which indicates the huge impact of SST on the development of TC. Therefore, it is widely accepted that a higher SST is more favorable for the genesis of TC [16]. Webster et al. [17] examined the number and intensity of TCs in an environment of increasing SST, and their results revealed the positive correlation between the quantity of intense TCs and SST over the North Pacific, Indian, and Southwest Pacific Oceans. In addition, some numerical experiments also revealed the correlation between ocean surface and TC activities from various mechanisms [18–20].

However, as most of current TC research studies pay close attention only to the SST to characterize the contribution of the ocean, the ocean subsurface has received far less attention, and the influence of the ocean subsurface is often skipped over arbitrarily. The energy of a TC is supplied by the warm preexisting underlying ocean, however, as a TC gains energy, the cooling of sea surface is unavoidable due to

both the energy transferred by strong turbulent fluxes at the sea surface and the vertical mixing of upwelling cooler subsurface water with the warm surface water in the ocean subsurface [21, 22]. The strength of this effect depends on the ocean subsurface thermal structure, as well as the TC translation speed, size, and wind speed [23–27], which is much stronger than the effect of aforementioned turbulent fluxes at the sea surface [23]. Effects of ocean subsurface on TC activities have been verified in several research studies. Guo and Tan [28] suggested that the rapid intensification of TC is strongly affected by upper ocean heat content, and Lin et al. [29] pointed out that subsurface ocean warming may contribute a lot to the genesis and intensification of supertyphoon. Furthermore, subsurface water temperature, which decides the vertical thermal structure of the ocean, may be responsible for the increase in frequency and intensity of El Niño and La Niña events [30, 31], which affects the large-scale atmospheric conditions and TC activities. According to the powerful influence of the ocean subsurface on the energy transfer during the genesis and intensification of TC, a survey on the relationship between the ocean subsurface and TC activities is of great significance.

The paper is organized as follows. Section 2 describes the data and methods used, and a brief analysis of the relationship between ocean subsurface and TCs activities over the WNP as well as a list of the subsurface cold years and warm years is presented in this section. Section 3 gives a statistical analysis of differences in genesis frequency, lifespan, and genesis position of TCs between subsurface cold and warm years. Section 4 discusses the responsible mechanism for the observed differences of TCs activities between subsurface cold and warm years, which is followed by conclusions and discussion in Section 5.

2. Data and Methodology

2.1. Data. In the present study, we use the TC best-track data from the Joint Typhoon Warning Centre [32]. The dataset contains the locations of the TC central position (latitudes and longitudes) and intensities (the maximum 1-minute mean sustained 10-meter wind speed) at six-hour intervals. The dataset over the WNP is available from 1945 to 2017. TCs having a tropical storm (TS, TC with maximum sustained wind speed of 33 knots or more) intensity or greater are included in our research. In addition, in order to distinguish TCs with a higher intensity, category 4 and 5 TCs (C45 TCs, TC with maximum sustained wind speed of 114 knots or more) are often presented separately. Owing to the inconsistent intensity estimate techniques and different computation methods, there exist some uncertainty and inconsistency in TC data among different agencies [33, 34]. For completeness, TC best-track data from the China Meteorological Administration Shanghai Typhoon Institute (CMASTI) [35] is also taken into account.

From the subsurface temperature and salinity analysis dataset produced by Japan Agency for Marine-Earth Science and Technology (JAMSTEC) [36], monthly objectively analysed global ocean subsurface temperature information at 24 levels in the upper 1500 meters from 1948 to 2012 is acquired.

The monthly air temperature, mean wind, relative humidity, relative vorticity, and longwave radiation at the sea surface field and sea-level pressure (SLP) field from 1948 to 2017 are provided by the National Centers for Environmental Prediction (NCEP) and National Centre for Atmospheric Research (NCAR) reanalysis dataset [37]. In addition, monthly SST data is obtained from Hadley Centre Sea Ice and Sea Surface Temperature (HadISST) datasets [38]. Considering the time range of different datasets, monthly data from 1948 to 2012 is used in our research.

2.2. Methodology. There are 1667 TCs with intensities exceeding TS across the whole WNP basin from 1948 to 2012 (based on JTWC best-track dataset) (Figure 1). Figure 1 shows that the genesis positions of TCs over the WNP mainly locate in the following area: 0°–30°N, 100°–180°E. Therefore, the ocean subsurface temperature of this area is selected to study the relationship between subsurface and TC activities over the WNP. Many research studies have shown that upper subsurface with a depth of 100–150 m has a great impact on the energy supply for a TC [24, 39, 40], and the temperature of this layer over the WNP varies significantly on the interannual scale [41, 42]; hence, we choose the water temperature of the 125 m deep layer as a proxy to investigate the effects of ocean subsurface on TCs.

The correlation between seasonal mean subsurface water temperature and TC genesis frequency (TCF) during the peak TC season (June-November, hereafter JASON) from 1948 to 2012 over the WNP is examined firstly (Figure 2). Despite the inconsistency between different TC best-track datasets, the results show that both TCF and C45 TCF have a negative correlation with subsurface water temperature. A similar result is obtained using the EN4 quality controlled ocean data (EN.4.2.1) from the Hadley Centre subsurface temperature and salinity objective analyses [43]; since the result is qualitatively the same as the result from Ishii dataset, it is not shown here. However, as mentioned in Section 1, a warmer ocean surface tends to induce more TC activities; the ocean surface and subsurface showed different correlation with TC activities.

As the essential roles of SST in the TC activities over the WNP [44], the correlation between SST and ocean subsurface temperature is analysed. Figure 3 demonstrates the spatial distribution of correlation coefficient between JASON seasonal averaged SST and ocean subsurface temperature; subsurface temperature shows different correlation with SST in different position, and a negative correlation centre locates in the southeastern WNP, while other areas show a positive correlation. This means a warmer subsurface does not always correspond to a warmer surface, and the ocean subsurface may have different characteristic from the surface. Hence, analysis on the relationship between ocean subsurface temperature and TC activities is not simply an extrapolation of the relationship between SST and TC activities; it may provide a distinctive help for understanding the mechanism of TC activity over the WNP.

The linkage between ENSO and TC activity should also be surveyed as ocean subsurface temperature over the WNP

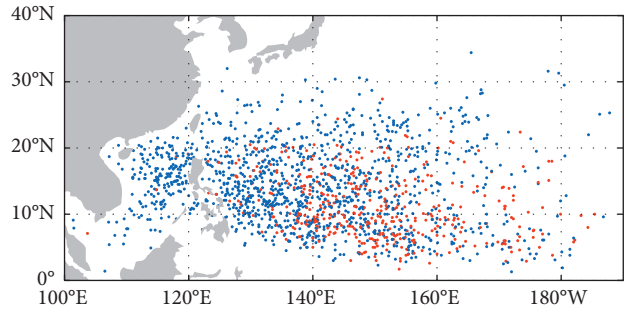

Figure 1: Spatial distribution of genesis positions of all TCs over the WNP. Blue dots denote the genesis positions of TCs with intensities reaching TS, and red dots denote the genesis positions of C45 TCs.

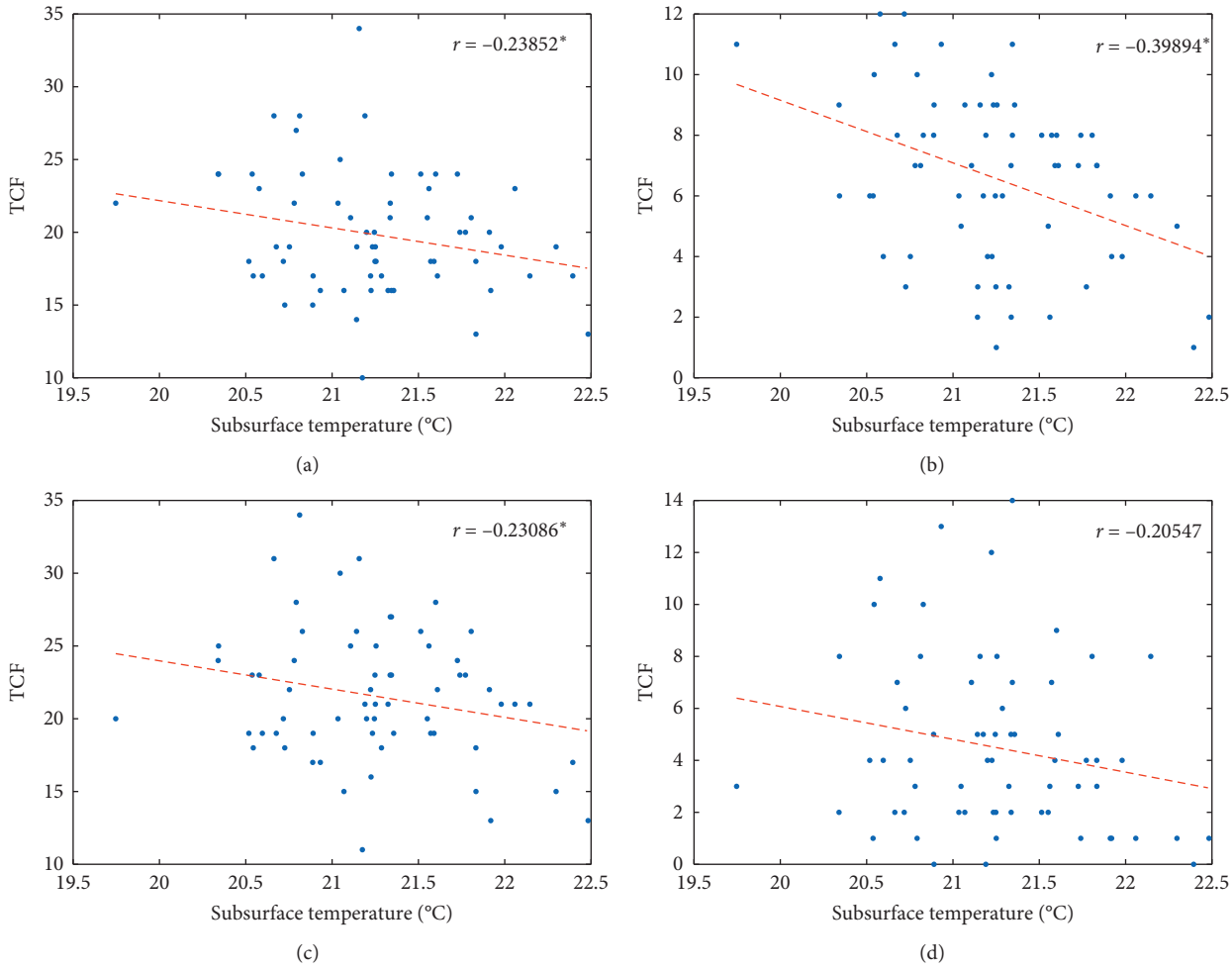

Figure 2: Scatter plots of observed (a) TCF from JTWC dataset, (b) C45 TCF from JTWC dataset, (c) TCF from CMASTI dataset, and (d) C45 TCF from CMASTI dataset from mean subsurface temperature during JASON season. The red-dotted line is the linear fitting curve, r is the correlation coefficient between TCF and mean subsurface temperature during JASON season, and the superscript $*$ indicates that the correlation is statistically significant at the 90% confidence level.

is highly related to the ENSO cycle. We calculated the correlation coefficient between the annual Niño3.4 SST index and TCF, and there is no obvious direct correlation between them ($r = -0.0076$); the correlation between ocean subsurface temperature and TCF ($r = -0.2385$, Figure 2(a)) is more significant than this. Although the impact of ENSO on TC activity has been demonstrated by many studies [45], the correlation between ocean subsurface temperature and TC activity may provide some new information on the TC activity over the WNP.

To further determine the negative correlation between TCF and ocean subsurface temperature and to investigate

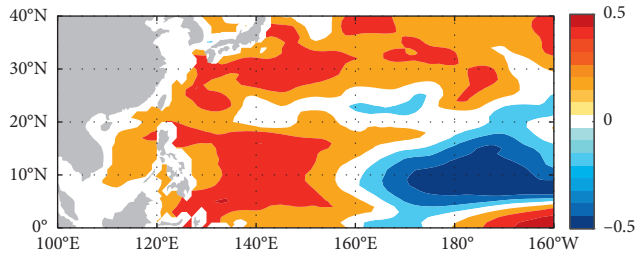

Figure 3: Distribution of correlation coefficient between JASON seasonal averaged SST and ocean subsurface temperature.

how this correlation is formed, we calculated the average water temperature of the 125 m deep layer in the area of 0°–30°N, 100°–180°E during JASON season annually (Figure 4). It should be noted that the cold and warm years in this study are defined as follows: the detrended subsurface temperature anomalies are larger than 0.5°C for the warm years and lower than −0.5°C for the cold years. The selected subsurface warm and cold years are shown in Table 1.

3. Statistical Analysis

3.1. TCF. To examine the decreasing trend in TCF with the rise of subsurface temperature shown in Figure 2, we calculated the mean JASON seasonal TCF annually based on both JTWC and CMASTI TC best-track datasets (Table 2). The annual TCF is 21.57 in JTWC dataset and 22.50 in CMASTI dataset during JASON season of the subsurface cold years and 18.50 in JTWC dataset and 19.20 in CMASTI dataset during the warm years. The differences between warm and cold years are 3.07 and 3.30 from JTWC dataset and CMASTI dataset, respectively. Both of the differences are statistically significant at the 95% confidence level. During JASON season of subsurface cold years, C45 TCF is 8.29 in JTWC dataset and 4.43 in CMASTI dataset, and during JASON of subsurface warm years, C45 TCF is 4.50 in JTWC dataset and 2.90 in CMASTI dataset. Despite the inconsistency of C45 TCF between two datasets caused by different recording methods, intense TCs formed much more frequently in the cold years than in the warm years, the former is almost twice the value of the latter, and only the difference from the JTWC dataset is statistically significant.

We further divided the WNP basin into four quadrants, and (150°E, 15°N) was selected as the origin for the four quadrants following Chen and Tam [46]. The comparison of the average TCF in four quadrants is shown in Figure 5. Note that C45 TCF had not been analysed because the value of averaged C45 TCF in four separate quadrants was too small to compare. The TCFs in southwestern and northeastern quadrants showed no significant difference between subsurface cold and warm years, as the difference mainly came from northwestern and southeastern quadrants. For the northwestern quadrant, the averaged TCF in JASON season was 4.5 in cold years and 7.8 in warm years from JTWC dataset (and 6.1 in cold years and 8.4 in warm years from CMASTI dataset). Thus, there were more TCs generated in northwestern quadrant in subsurface warm years than in cold years. The difference between cold and warm years is statistically significant at the 95% confidence level. For the southeastern quadrant, TCs rarely generated in this quadrant in warm years. The averaged TCF in JASON season is 8.6 in cold years and 1.2 in warm years from JTWC dataset (6.6 in cold years and 0.7 in warm years from CMASTI dataset), and the difference between cold and warm years is also statistically significant at the 95% confidence level. Therefore, the negative correlation between TCF and subsurface water temperature shown in Section 2.2 is mainly caused by the difference of TCF in the southeastern quadrant.

3.2. Lifespan of TC. We further examined the lifespan of TCs in the subsurface cold and warm years separately, and the results are shown in Table 3. Despite the inconsistency of mean lifespan between two datasets caused by different estimate techniques and computation methods, an obvious difference can be observed in the mean lifespan of TCs during JASON season between subsurface cold and warm years. In the JTWC dataset, mean lifespan of TCs in cold years is 241.49 h, which is more than double of the value in the warm years (106.31 h), and the difference (135.18 h) is statistically significant at the 95% confidence level. Similar results can be derived from the CMASTI dataset: 201.79 h in the cold years and 97.62 h in the warm years; thus the difference (104.17 h) is also significant. As for the C45 TCs, the difference in lifespan is even more prominent, and the lifespan of C45 TCs in subsurface cold years is about three times that of the warm years (328.81 h in cold years and 108.31 h in warm years from JTWC dataset and 292.5 h in cold years and 115.85 h in warm years from CMASTI dataset). In addition, it is noteworthy that the difference of duration between C45 TCs and normal TCs in cold years is much greater than that of the warm years, which indicates that intense TC generated in subsurface cold years tends to have a longer lifespan.

4. Diagnosis of Environmental Factors

To understand the mechanism responsible for the statistical relationship between ocean subsurface and TCs activities over the WNP demonstrated in Section 3, we analysed the impacts of environmental factors on TCs activities using two genesis potential indexes (GPI).

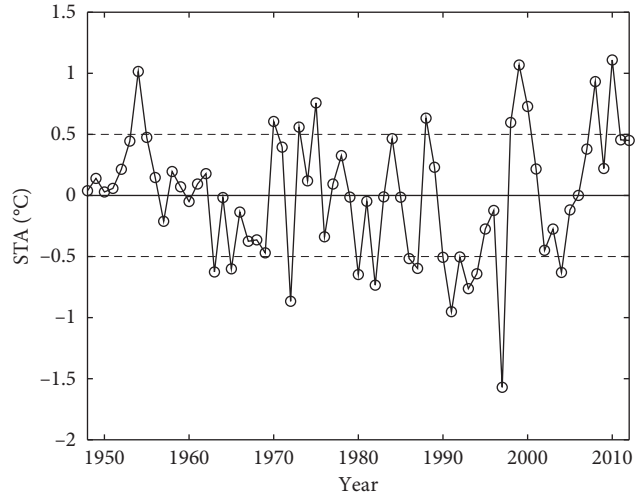

Figure 4: Interannual variations of the detrended subsurface temperature anomalies of the 125 m deep layer in the area of 0°–30°N, 100°–180°E during JASON season.

Table 1: List of the subsurface cold years and warm years during 1948–2012.

Subsurface cold years	Subsurface warm years
1963, 1965, 1972, 1980, 1982, 1986, 1987, 1990, 1991, 1992, 1993, 1994, 1997, 2004 (14)	1954, 1970, 1973, 1975, 1988, 1998, 1999, 2000, 2008, 2010 (10)

Table 2: Mean TCF generated during JASON season in the subsurface warm year and cold year.

	TCF			C45 TCF		
	Cold years	Warm years	Diff (cold-warm)	Cold years	Warm years	Diff (cold-warm)
JTWC	21.57	18.50	3.07*	8.29	4.50	3.79*
CMASTI	22.50	19.20	3.30*	4.43	2.90	1.53

*The difference is statistically significant at the 95% confidence level.

4.1. GPI. The TC GPI is a widely used parameter to diagnose impact factors of TC genesis [47], which is calculated based on the empirical equation by Emanuel and Nolan [48] (referred to as GPI_{04} hereafter) as given below:

$$\mathrm{GPI}_{04} = \underbrace{\left|10^5\eta\right|^{(3/2)}}_{\text{Term1}} \underbrace{\left(\frac{H}{50}\right)^3}_{\text{Term2}} \underbrace{\left(\frac{V_{\text{pot}}}{70}\right)^3}_{\text{Term3}} \underbrace{\left(1 + 0.1V_{\text{shear}}\right)^{-2}}_{\text{Term4}}, \tag{1}$$

where η is the absolute vorticity at 850 hPa (s^{-1}), H is the relative humidity at 600 hPa (%), and V_{pot} is the maximum TC potential intensity (PI, $\mathrm{m}\cdot\mathrm{s}^{-1}$) defined by Emanual et al. [49–51]:

$$V_{\text{pot}}^2 = C_p\left(T_s - T_o\right)\frac{T_s}{T_o}\frac{C_k}{C_D}\left(\ln\theta_e^* - \ln\theta_e\right), \tag{2}$$

where C_p denotes the heat capacity at constant pressure, T_s is the SST, T_o is the temperature of TC outflow, C_k is the exchange coefficient for enthalpy, C_D is the drag coefficient, θ_e^* is the saturation equivalent potential temperature at the ocean surface, and θ_e is the equivalent potential temperature in the boundary layer. A FORTRAN subroutine to calculate PI is available online (http://wind.mit.edu/~emanuel/home.html),V_{shear} is the vertical wind shear ($\mathrm{m}\cdot\mathrm{s}^{-1}$), which is defined as

$$V_{\text{shear}} = \sqrt{\left(u_{200} - u_{850}\right)^2 + \left(v_{200} - v_{850}\right)^2}, \tag{3}$$

where u_{200} and u_{850} represent the zonal wind speeds at 200 hPa and 850 hPa, and v_{200} and v_{850} are the meridional wind speeds at 200 hPa and 850 hPa, respectively.

To include the impact of ocean subsurface on the TC genesis, we also adapt another TC genesis potential index which considers oceanic parameters (referred to as $\mathrm{GPI}_{\text{ocean}}$ hereafter) [52]:

$$\mathrm{GPI}_{\text{ocean}} = \underbrace{\left|10^5\eta_{1000}\right|^{0.9}}_{\text{Term1}} \underbrace{\left(\frac{\overline{T}}{26}\right)^{7.64}}_{\text{Term2}} \underbrace{\left(\frac{F}{45}\right)^{-2.73}}_{\text{Term3}} \underbrace{\left(\frac{D_{26}}{80}\right)^{0.25}}_{\text{Term4}}, \tag{4}$$

where η_{1000} is the absolute vorticity at 1000 hPa (s^{-1}), $\overline{T}$ is the mean temperature in the ocean mixed layer (°C; in this study, the mixed layer depth is defined as the depth where the temperature is smaller than the temperature at 5 m depth by 0.2°C, following Thompson [53]), F is the net longwave

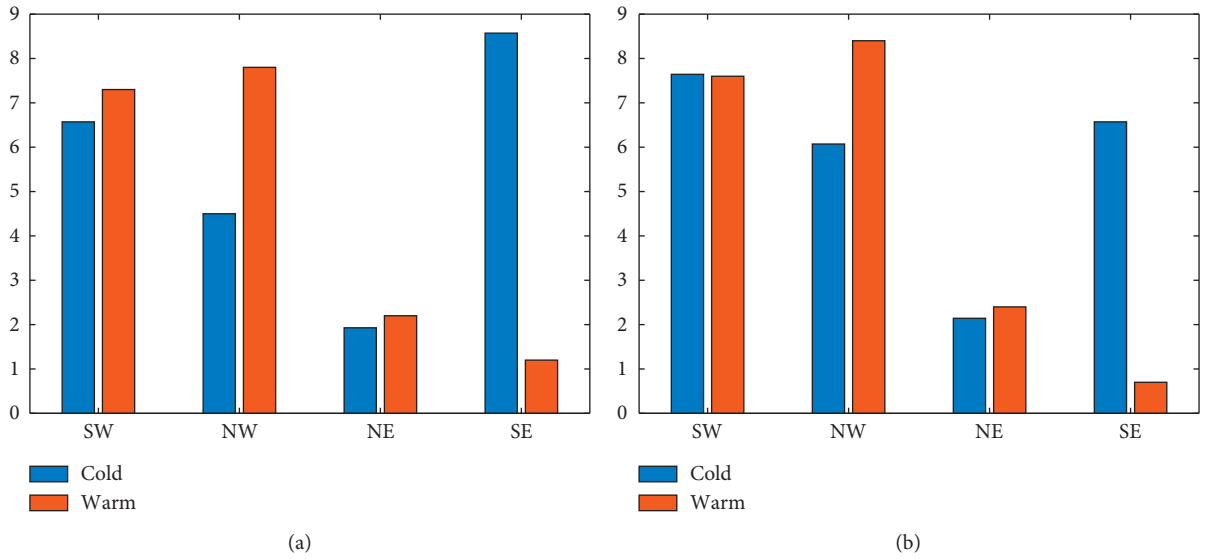

Figure 5: The average TCF in four quadrants from (a) JTWC dataset and (b) CMASTI dataset during JASON season.

Table 3: Mean TC lifespan during JASON season in the subsurface cold and warm years.

	TC lifespan (h)			C45 TC lifespan (h)		
	Cold years	Warm years	Diff (cold-warm)	Cold years	Warm years	Diff (cold-warm)
JTWC	241.49	106.31	135.18*	323.81	108.31	215.50*
CMASTI	201.79	97.62	104.17*	292.50	115.85	176.68

*The difference is statistically significant at the 95% confidence level.

radiation at the sea surface ($W \cdot m^{-2}$, positive radiation is upward), and D_{26} is the depth of the 26°C isotherm (m).

Figure 6 displays the composite difference of GPI between subsurface cold and warm years in JASON season. The distribution of difference of GPI_{04} and GPI_{ocean} is similar in general. The GPI difference positive areas locate in the southeast of the WNP basin for both GPI_{04} and GPI_{ocean}, which implies that the southeast WNP basin is more favorable for the genesis of TC in the subsurface cold years than in the warm years. The negative centre locates in the East China Sea; due to the relatively high latitude, this negative centre cannot induce an obvious higher frequency of TC activities in the subsurface warm years. As mentioned above, the result of the composite difference of GPI is consistent with the statistically analytical result of TC genesis position in Section 3.1, which denotes that the impact factors of the relationship between ocean subsurface and TCs activities over the WNP are captured well in both the GPI_{04} and GPI_{ocean} analyses.

4.2. Relative Contributions of Environmental Variables. To further determine the relative contributions of each environmental factor to results in Section 4.1, the main TC genesis area of the southeastern quadrant (0°–15°N, 150°–180°E, i.e., the dashed rectangle in Figure 6) is selected for analysis. We divided GPI_{04} (GPI_{ocean}) into four separate parts as in Equation (1): Term1 came from the 850 hPa absolute vorticity (the 1000 hPa absolute vorticity for GPI_{ocean}), Term2 from the 600 hPa relative humidity (the mean temperature in the ocean mixed layer for GPI_{ocean}), Term3 from the maximum PI (the net longwave radiation at the sea surface for GPI_{ocean}), and Term4 from the 200–850 hPa vertical wind shear (the depth of the 26°C isotherm for GPI_{ocean}). Following Li et al. [54], taking a natural logarithm on both sides of Equation (1),

$$\begin{aligned} \ln \mathrm{GPI} &= \ln(\mathrm{Term1} \times \mathrm{Term2} \times \mathrm{Term3} \times \mathrm{Term4}) \\ &= \ln(\mathrm{Term1}) + \ln(\mathrm{Term2}) + \ln(\mathrm{Term3}) \\ &\quad + \ln(\mathrm{Term4}). \end{aligned} \tag{5}$$

Then, applying a total differential at both sides of Equation (5),

$$\frac{d\mathrm{GPI}}{\mathrm{GPI}} = \frac{d\mathrm{Term1}}{\mathrm{Term1}} + \frac{d\mathrm{Term2}}{\mathrm{Term2}} + \frac{d\mathrm{Term3}}{\mathrm{Term3}} + \frac{d\mathrm{Term4}}{\mathrm{Term4}}. \tag{6}$$

By substituting Equation (6) into Equation (1), we get

$$\begin{aligned} d\mathrm{GPI} &= d\mathrm{Term1} \times \mathrm{Term2} \times \mathrm{Term3} \times \mathrm{Term4} + d\mathrm{Term2} \times \mathrm{Term1} \\ &\quad \times \mathrm{Term3} \times \mathrm{Term4} + d\mathrm{Term3} \times \mathrm{Term1} \times \mathrm{Term2} \\ &\quad \times \mathrm{Term4} + d\mathrm{Term4} \times \mathrm{Term1} \times \mathrm{Term2} \times \mathrm{Term3}. \end{aligned} \tag{7}$$

By integrating Equation (7) from subsurface warm year to cold year, we have

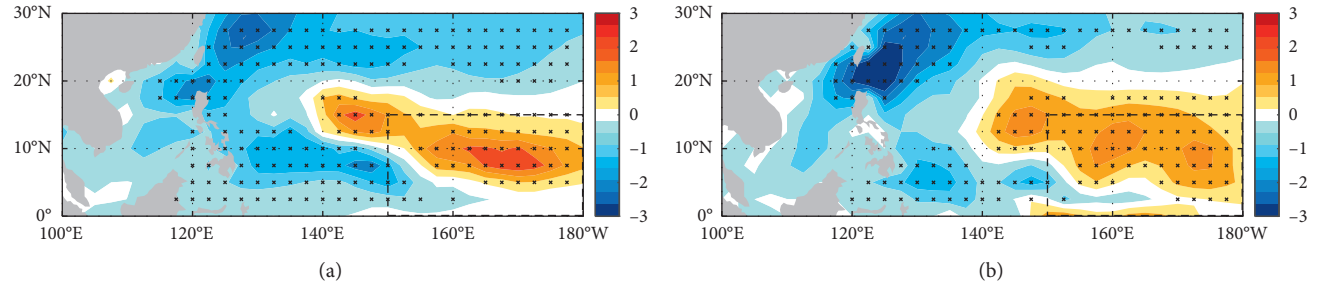

Figure 6: The composite difference of (a) GPI_{04} and (b) GPI_{ocean} between subsurface cold and warm years in JASON season (cold-warm). The cross sign indicates that the difference is statistically significant at the 95% confidence level.

$$\delta GPI_{w\longrightarrow c} = \delta GPI_c - \delta GPI_w = \left(GPI_c - \overline{GPI}\right) - \left(GPI_w - \overline{GPI}\right), \tag{8}$$

where $\delta GPI_{w\longrightarrow c}$ denotes the difference between the subsurface warm year and cold year, δGPI_c indicates the difference between the subsurface cold year and the climatological mean, δGPI_w is the difference between the subsurface warm year and the climatological mean, and a bar means the climatological mean value. δGPI_c and δGPI_w can be written as

$$\delta GPI_c = GPI_c - \overline{GPI} = \alpha_1 \times \delta Term1_c + \alpha_2 \times \delta Term2_c + \alpha_3 \times \delta Term3_c + \alpha_4 \times \delta Term4_c, \tag{9}$$

$$\delta GPI_w = GPI_w - \overline{GPI} = \alpha_1 \times \delta Term1_w + \alpha_2 \times \delta Term2_w + \alpha_3 \times \delta Term3_w + \alpha_4 \times \delta Term4_w. \tag{10}$$

Substituting Equations (9) and (10) into Equation (8), we get

$$\delta GPI_{w\longrightarrow c} = \alpha_1 \times \left(\delta Term1_c - \delta Term1_w\right) + \alpha_2 \times \left(\delta Term2_c - \delta Term2_w\right) + \alpha_3 \times \left(\delta Term3_c - \delta Term3_w\right) + \alpha_4 \times \left(\delta Term4_c - \delta Term4_w\right). \tag{11}$$

And

$$\begin{cases} \alpha_1 = \overline{Term2} \times \overline{Term3} \times \overline{Term4}, \\ \alpha_2 = \overline{Term1} \times \overline{Term3} \times \overline{Term4}, \\ \alpha_3 = \overline{Term1} \times \overline{Term2} \times \overline{Term4}, \\ \alpha_4 = \overline{Term1} \times \overline{Term2} \times \overline{Term3}, \end{cases} \tag{12}$$

and here an approximation has been made by assuming α_1, α_2, α_3, and α_4 as constant coefficients. Figure 7 shows the diagnosis results of δGPI in the southeastern quadrant in subsurface cold years from Equation (9), warm years from Equation (10), and the difference between them from Equation (11). Different color bars denote the relative contributions of four environmental factors to TC genesis. For GPI_{04}, from the first column of Figure 7(a), the positive anomalies of GPI in cold year mainly come from Term1 (or the contribution of 850 hPa absolute vorticity). Meanwhile, from the second column, all four terms contribute to the negative anomalies of GPI in warm years, in which Term1, Term2, and Term4 play a major role among them. From the last column, the difference of δGPI_{04} between subsurface cold and warm years is also mainly related to Term1, Term2, and Term4 (or the contribution of 850 hPa absolute vorticity, 600 hPa relative humidity, and 200–850 hPa vertical wind shear, respectively). For GPI_{ocean}, from the first column of Figure 7(b), the positive anomalies of GPI in cold year mainly come from Term1 and Term3 (or the contribution of 1000 hPa absolute vorticity and net longwave radiation, respectively). Meanwhile, from the second column, Term1, Term2, and Term3 contribute to the negative anomalies of GPI in warm years (or the contribution of the 1000 hPa absolute vorticity, the mean temperature in the ocean mixed layer, and the net longwave radiation, respectively). From the last column, the difference of δGPI_{ocean} between subsurface cold and warm years is also mainly attributed to the 1000 hPa absolute vorticity, the mean temperature in the ocean mixed layer, and the net longwave radiation. Furthermore, it is shown in Figure 7(b) that the depth of the 26°C isotherm (Term4) makes a negative contribution in the subsurface cold years and a positive contribution in the subsurface warm years to the TC genesis, which is consistent with our understanding that warmer ocean will induce more TC activities, but this term did not play a dominant role in the δGPI analysis, and the contribution of it had been offset by other terms.

The environmental factors that have influence on TC genesis are shown in Figures 8 and 9. Figure 8 shows the composite anomalies of 850 hPa absolute vorticity, relative humidity, and vertical wind shear during JASON season in the subsurface cold and warm years and their difference. From the anomalies of absolute vorticity (Figures 8(a)–8(c)), the distribution of them over the WNP during subsurface cold and warm years is approximately opposite. Specifically, large positive absolute vorticity anomalies are observed in 5°–20°N basin during subsurface cold years, which covers the major area of southeastern and southwestern quadrant, and negative anomalies are mainly located near the equator.

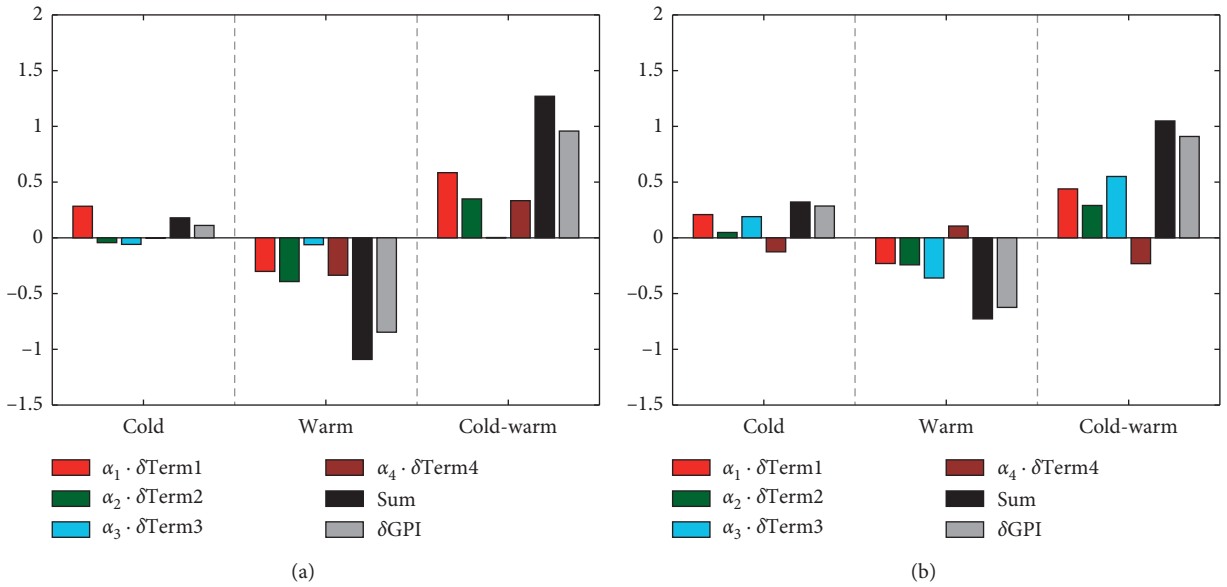

Figure 7: Relative contributions to (a) δGPI_{04} and (b) $\delta\text{GPI}_{\text{ocean}}$ of four terms on the right-hand sides of Equations (9)–(11), their sum, and the observed δGPI.

Contrary to the subsurface warm years, 5°–20°N basin is mainly controlled by negative anomalies; thus, from the contour map of difference between subsurface cold and warm years, positive values of difference are presented in the major area of the WNP. For anomalies of relative humidity (Figures 8(d)–8(f)), weak negative anomalies are presented over the most area of the WNP, but no obvious signals were observed over southeastern quadrant during cold years. However, during subsurface warm years, negative anomalies are observed over southeastern quadrant, which induces positive values of difference over southeastern quadrant. In addition, for anomalies of vertical wind shear (Figures 8(g)–8(i)), large positive anomalies are captured over the western Pacific warm pool region, and a negative centre locates in the east of it during subsurface cold years, but distribution of anomalies in warm years is roughly the opposite; both positive and negative values of difference are presented over the main TC genesis area of southeastern quadrant.

Figure 9 shows the composite anomalies of the 1000 hPa absolute vorticity, the mean temperature in the ocean mixed layer, the net longwave radiation at the sea surface and the depth of the 26°C isotherm during JASON season in subsurface cold and warm years and their difference. For the anomalies of the 1000 hPa absolute vorticity (Figures 9(a)–9(c)), the distribution of it is similar to the 850 hPa absolute vorticity shown in Figures 8(a)–8(c). From the anomalies of the mean temperature in the ocean mixed layer (Figures 9(d)–9(f)), it is shown that the phase of the mean temperature in the Central Pacific mixed layer is opposite to the phase of subsurface temperature in the WNP, and there is a positive anomalies centre in the area of 170°E–160°W, 10°S–10°N during the subsurface cold years and a negative anomalies centre during the subsurface warm years; therefore the contribution of $\overline{T}$ in Figure 7(b) is caused by this. For the anomalies of the net longwave radiation at the sea surface (Figures 9(g)–9(i)), negative anomalies are presented over the most area of the WNP during the subsurface cold years; however, the southeast of the WNP basin is covered by positive anomalies, resulting in a negative difference (or a positive contribution in Figure 7(b)) in the southeastern quadrant. In addition, for anomalies of D_{26} (Figure 9(j)–9(l)), the distribution of D_{26} is consistent with the ocean subsurface temperature, and the subsurface cold years tend to have a deeper D_{26} than the warm years.

In summary, the results shown in Figures 8 and 9 match the results from GPI analysis (Figure 7) well. To be specific, composite distribution of environmental factors differs greatly between subsurface cold and warm years. For the southeastern quadrant, where the TC genesis showed a huge difference between subsurface cold and warm years, three parameters from GPI_{04}, 850 hPa absolute vorticity, 600 hPa relative humidity, and 200–850 hPa vertical wind shear, have promoting effects on the difference; the contribution of maximum TC PI in GPI_{04} is not obvious. All four parameters from $\text{GPI}_{\text{ocean}}$ contribute to the difference of TC genesis in the southeastern quadrant. Three of them (1000 hPa absolute vorticity, mean temperature in the ocean mixed layer, and net longwave radiation at the sea surface) have positive effects on the difference, while the term of D_{26} has a negative effect but was offset by other terms.

Therefore, we can draw the conclusion that ocean subsurface water temperature has a close relationship with the TC activities over the WNP; this relationship was established based on the linkage between ocean

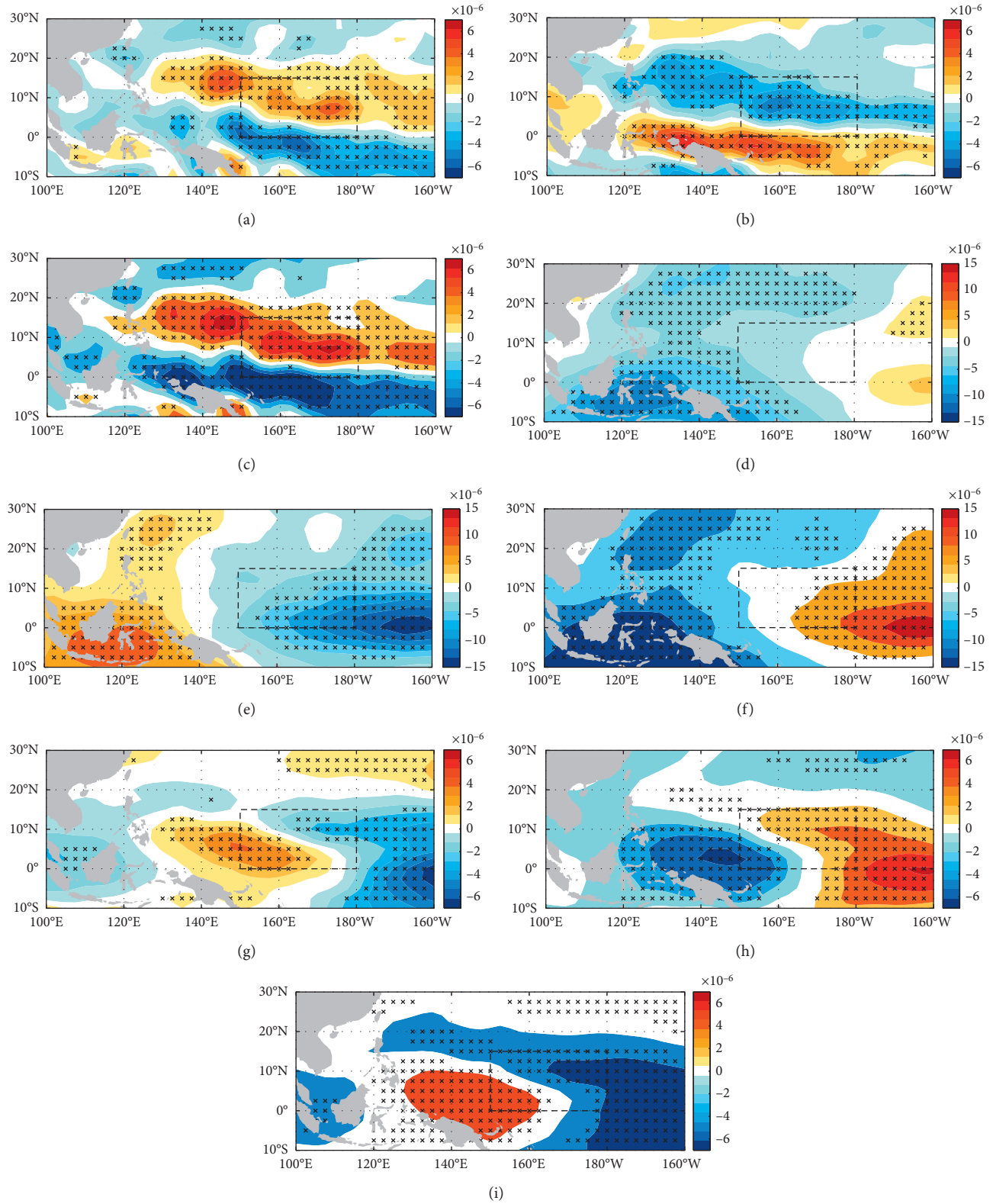

Figure 8: Composite anomalies of (a) absolute vorticity (units: s^{-1}), (d) relative humidity (units: %), and (g) vertical wind shear (units $m \cdot s^{-1}$) in JASON season for the subsurface cold years; (b), (e), and (h) as in (a), (d), and (g), but for the subsurface warm years; (c), (f), and (i) for the difference of composite anomalies between subsurface cold and warm years (cold-warm). Dashed rectangle indicates the main TC genesis area of southeastern quadrant mentioned in Section 4.2. The cross signs indicate that the values are statistically significant at the 95% confidence level.

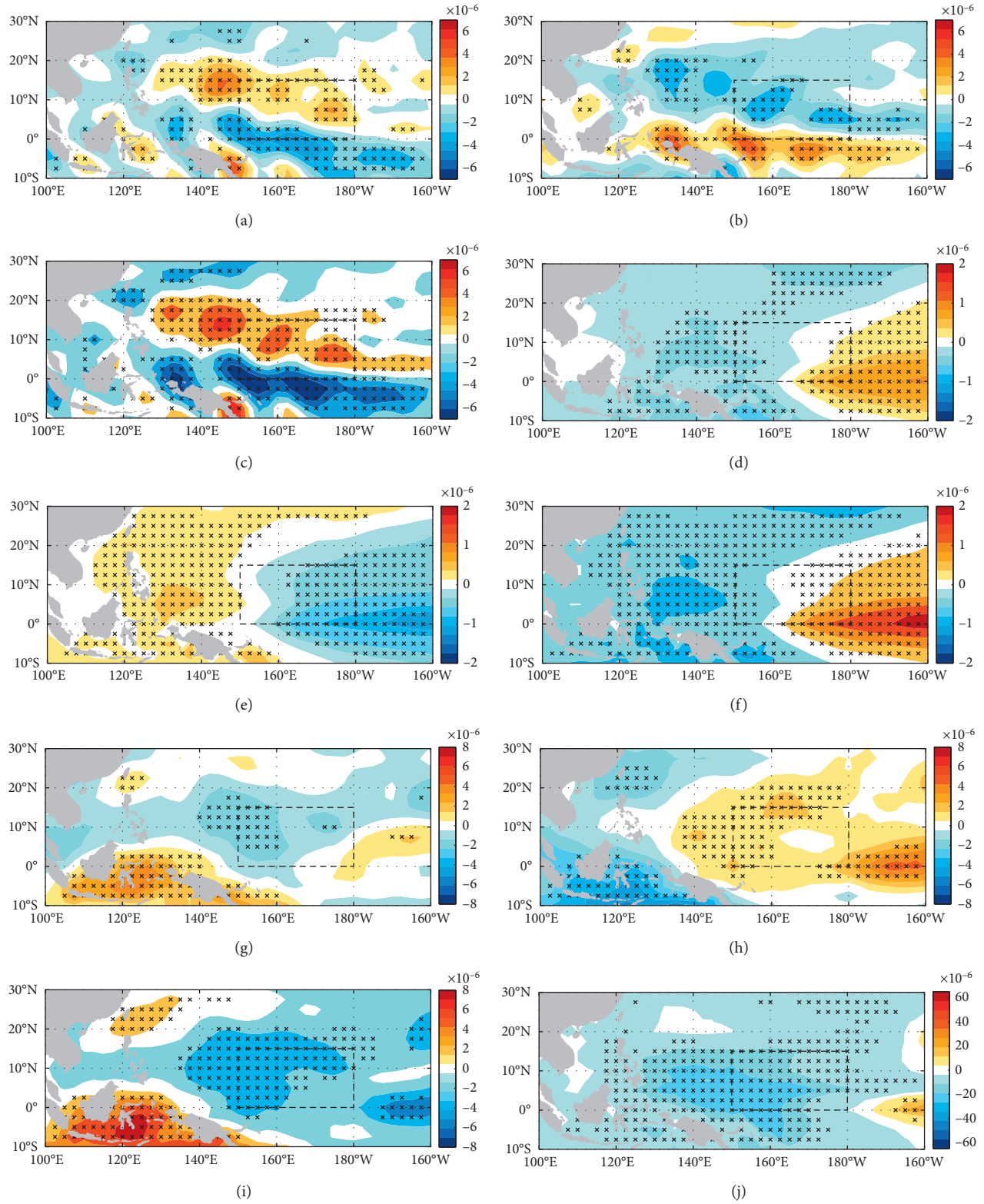

Figure 9: Continued.

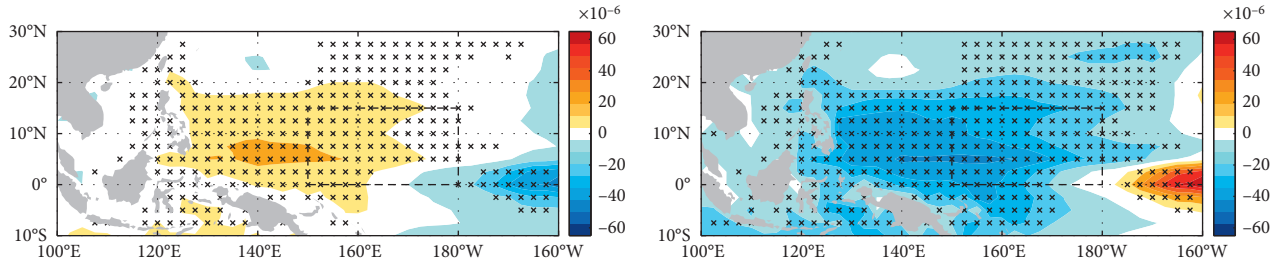

Figure 9: Composite anomalies of (a) the 1000 hPa absolute vorticity (units: s^{-1}), (d) the mean temperature in the ocean mixed layer (units: °C), (g) the net longwave radiation at the sea surface (units: $W \cdot m^{-2}$), and (j) the depth of 26°C isotherm (units: m) in JASON season for the subsurface cold years; (b), (e), (h), and (k) as in (a), (d), (g), and (j), but for the subsurface warm years; (c), (f), (i), and (l) for the difference of composite anomalies between subsurface cold and warm years (cold-warm). Dashed rectangle indicates the main TC genesis area of southeastern quadrant mentioned in Section 4.2. The cross signs indicate that the values are statistically significant at the 95% confidence level.

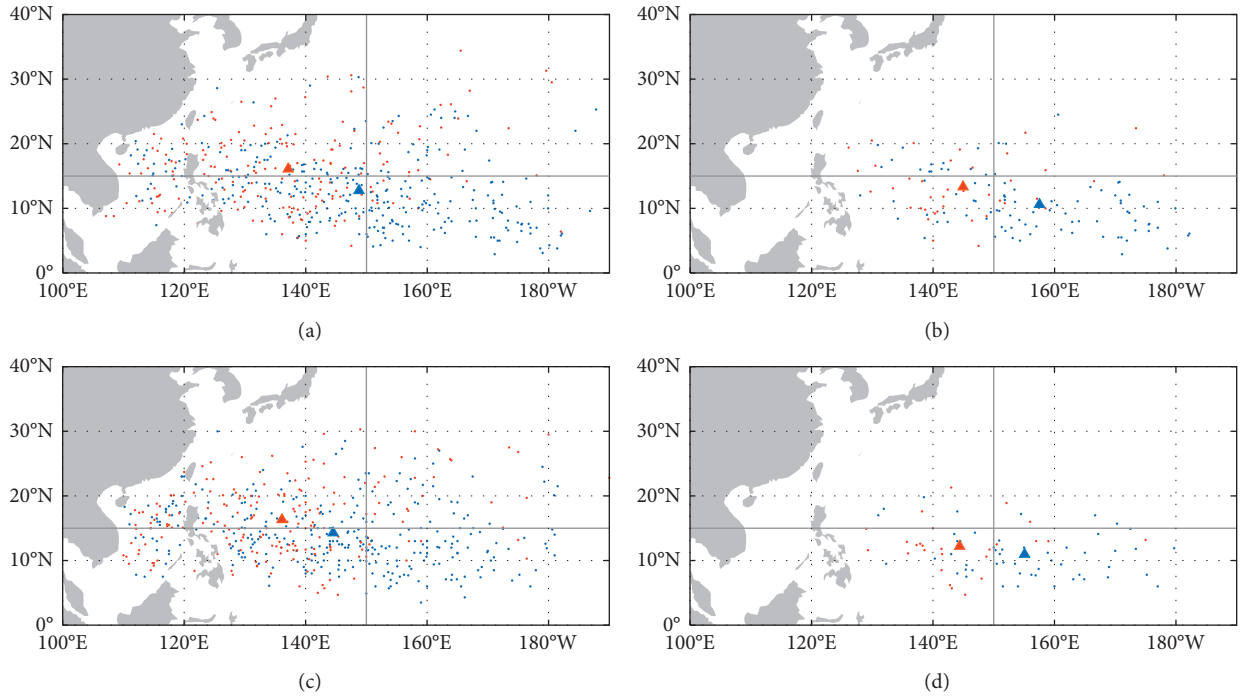

Figure 10: Genesis positions of (a) TCs in JTWC dataset, (b) C45 TCs in JTWC dataset, (c) TCs in CMASTI dataset, and (d) C45 TCs in CMASTI dataset during JASON season. The solid line denotes the boundary line of four quadrants. Blue and red triangles indicate the mean genesis positions of TCs in cold and warm years, respectively.

subsurface and other oceanic or atmospheric parameters which have influence on the TC occurrence and development.

5. Conclusions and Discussion

In this study, we have investigated the relationship between ocean subsurface temperature and TC activities over the WNP basin during 1948–2012. A negative correlation between subsurface water temperature and TCF is observed (Figure 2). We have selected subsurface cold and warm years according to the water temperature of 125 m deep layer, and we found that more TCs occurred in subsurface cold years than in warm years (3.07 larger per year in JTWC dataset and 3.30 larger in CMASTI dataset on average), and the number of C45 TCs in the subsurface cold years is also larger than that in the warm years (3.79 larger per year in JTWC dataset and 1.53 larger per year in CMASTI dataset on average). By dividing the WNP basin into four quadrants, we found that the differences in TCF between cold and warm years mainly come from the southeast of the WNP, where there are much more TCs generated in the southeastern

quadrant in cold years than in warm years. Moreover, the differences in the lifespan and genesis position of TCs between cold and warm years are also significant. Specifically, TCs generated in cold years have a longer duration than in warm years (135.18 h longer in JTWC dataset and 104.17 h longer in CMASTI dataset on average), and the differences are even larger for the C45 TCs (215.50 h longer in JTWC dataset and 176.68 h longer in CMASTI dataset on average). The mean genesis position of both TCs and C45 TCs in cold years is more southeastern than warm years (Figure 10 and Table 3), which means that the genesis positions of TCs that occurred in cold years are farther from mainland than in warm years, resulting in a longer time to travel over the warm ocean, and thus have bigger chance to intensify. This can explain why TCs that occurred in cold years have a longer lifespan in general. All these suggest that ocean subsurface temperature has a nonnegligible effect on TC activities over the WNP basin.

By using the TC genesis potential indexes (GPI), the influence of the large-scale environmental factors on TC genesis is examined. A general diagnosis shows that both GPI_{04} and GPI_{ocean} can capture the major characteristics of TC generated well over the WNP. Moreover, both GPI_{04} and GPI_{ocean} index can be divided into four separate terms to denote the individual influence of environmental factors. For GPI_{04}, four terms are the absolute vorticity (850 hPa), the relative humidity, the maximum TC PI, and the vertical wind shear, and for GPI_{ocean}, they are the absolute vorticity (1000 hPa), the mean temperature in the ocean mixed layer, the net longwave radiation, and the depth of 26°C isotherm. By doing this, we found that the variation of distribution of environmental factors from cold years to warm years is enormous, which contributes to the differences of TC activities. From the results of GPI_{04} analysis, compared with the subsurface warm years, the southeastern quadrant tends to have larger relative vorticity, higher relative humidity, and smaller vertical wind shear during cold years, which are favorable for genesis and development of TC. The difference of maximum TC PI between cold and warm years is not obvious. From the results of GPI_{ocean} analysis, compared with the subsurface warm years, the southeastern quadrant tends to have larger relative vorticity, higher temperature in the ocean mixed layer, and weaker net longwave radiation during cold years, which promote the genesis and development of TC. Moreover, the depth of 26°C isotherm is deeper in the subsurface cold years than in the warm years, which should have a promoting effect on the TC genesis in the warm years, but this effect was offset by other terms. Therefore, the relationship between ocean subsurface temperature and the TC activities over the WNP is verified from the TC GPI analysis; it is established based on the linkage between ocean subsurface and other oceanic or atmospheric parameters which have influence on the TC occurrence and development.

As a final remark, this study mainly focused on the relationship between ocean subsurface temperature and TC activities over the WNP; thus we should be cautious to only do some correlation analysis to explain their relationship; it is of great importance to survey it from the large-scale environment and to find out the physical mechanism beneath the correlation. In this study, we have denoted that subsurface conditions may have impacts on the atmospheric wind and moisture fields. We believe that further investigation into the approach of how ocean subsurface affects the atmosphere by data analysis or air-sea coupling numerical model is necessary.

Data Availability

(1) The JTWC TC Best-Track data used to support the findings of this study have been deposited in the Joint Typhoon Warning Centre website (https://www.metoc.navy.mil/jtwc/jtwc.html?western-pacific). (2) The CMA TC Best-Track data used to support the findings of this study have been deposited in the China Meteorological Administration Tropical Cyclone Database (https://doi.org/10.1175/JTECH-D-12-00119.1). (3) The JAMSTEC ocean subsurface temperature data used to support the findings of this study have been deposited in Japan Agency for Marine-Earth Science and Technology (https://doi.org/10.1002/joc.1169). (4) The EN4 ocean subsurface temperature data used to support the findings of this study have been deposited in Hadley Centre subsurface temperature and salinity objective analyses (https://doi.org/10.1002/2013JC009067). (5) The monthly air temperature, mean wind, relative humidity, relative vorticity, and longwave radiation at the sea surface field and sea-level pressure (SLP) field data used to support the findings of this study have been deposited in NCAR/NCEP reanalysis dataset (https://doi.org/10.1175/1520-0477(1996)077<0437:TNYRP>2.0.CO;2). (6) The monthly SST data used to support the findings of this study have been deposited in Hadley Centre Sea Ice and Sea Surface Temperature dataset (https://doi.org/10.1029/2002JD002670).

Conflicts of Interest

The authors declare that there are no financial or personal relationships with other people or organizations that can inappropriately influence their work. There is no professional or other personal interest of any nature or kind in any product, service, and/or company that could be construed as influencing the position presented in, or the review of, the manuscript entitled.

Acknowledgments

The efforts of the researchers who obtained and published the data used in this study, as well as their funding organizations, are much appreciated. This study was supported by the National Key Research and Development Program of China (Grant no. 2018YFB0203801) and the National Natural Science Foundation of China (Grant nos. 41605070, 61572510, 61702529, and 61802424)

References

[1] L. Yong and D. Chen, "An interdecadal change in the interannual variability of boreal summer tropical cyclone genesis frequency over the western North Pacific around the early 1990s," *Theoretical and Applied Climatology*, vol. 137, no. 3-4, pp. 1843–1853, 2019.

[2] Z. Zhong, X. Chen, X.-Q. Yang, Y. Ha, and Y. Sun, "The relationship of frequent tropical cyclone activities over the western North Pacific and hot summer days in central-eastern China," *Theoretical and Applied Climatology*, vol. 138, pp. 1395–1404, 2019.

[3] J.-W. Choi, Y. Cha, H.-D. Kim, and S.-D. Kang, "Latitudinal change of tropical cyclone maximum intensity in the western North Pacific," *Advances in Meteorology*, vol. 2016, Article ID 5829162, 8 pages, 2016.

[4] W. M. Gray and L. Brody, *Global View of the Origin of Tropical Disturbances and Storms*, Citeseer, Princeton, NJ, USA, 1967.

[5] T.-C. Chen, S.-P. Weng, N. Yamazaki, and S. Kiehne, "Interannual variation in the tropical cyclone formation over the western North pacific," *Monthly Weather Review*, vol. 126, no. 4, pp. 1080–1090, 1998.

[6] S. Yokoi, Y. N. Takayabu, and J. C. L. Chan, "Tropical cyclone genesis frequency over the western North Pacific simulated in medium-resolution coupled general circulation models," *Climate Dynamics*, vol. 33, no. 5, pp. 665–683, 2009.

[7] K. A. Emanuel, "An air-sea interaction theory forsss tropical cyclones. Part I: steady-state maintenance," *Journal of the Atmospheric Sciences*, vol. 43, no. 6, pp. 585–605, 1986.

[8] R. Rotunno and K. A. Emanuel, "An air-sea interaction theory for tropical cyclones. Part II: evolutionary study using a nonhydrostatic axisymmetric numerical model," *Journal of the Atmospheric Sciences*, vol. 44, no. 3, pp. 542–561, 1987.

[9] G. A. Vecchi and B. J. Soden, "Effect of remote sea surface temperature change on tropical cyclone potential intensity," *Nature*, vol. 450, no. 7172, pp. 1066–1070, 2007.

[10] P. J. Klotzbach, "Trends in global tropical cyclone activity over the past twenty years (1986–2005)," *Geophysical Research Letters*, vol. 33, no. 10, 2006.

[11] Z.-W. Zheng, "Unusual warming in the coastal region of northern South China Sea and its impact on the sudden intensification of tropical cyclone Tembin (2012)," *Advances in Meteorology*, vol. 2014, Article ID 250752, 7 pages, 2014.

[12] M. Mohapatra and V. V. Kumar, "Interannual variation of tropical cyclone energy metrics over North Indian Ocean," *Climate Dynamics*, vol. 48, no. 5-6, pp. 1431–1445, 2017.

[13] E. M. Vincent, M. Lengaigne, C. E. Menkes et al., "Interannual variability of the South Pacific Convergence Zone and implications for tropical cyclone genesis," *Climate Dynamics*, vol. 36, no. 9-10, pp. 1881–1896, 2011.

[14] K. A. Emanuel, "The dependence of hurricane intensity on climate," *Nature*, vol. 326, no. 6112, pp. 483–485, 1987.

[15] G. J. Holland, "The maximum potential intensity of tropical cyclones," *Journal of the Atmospheric Sciences*, vol. 54, no. 21, pp. 2519–2541, 1997.

[16] P.-S. Chu and J. D. Clark, "Decadal variations of tropical cyclone activity over the central North Pacific," *Bulletin of the American Meteorological Society*, vol. 80, no. 9, pp. 1875–1881, 1999.

[17] P. J. Webster, G. J. Holland, J. A. Curry, and H.-R. Chang, "Changes in tropical cyclone number, duration, and intensity in a warming environment," *Science*, vol. 309, no. 5742, pp. 1844–1846, 2005.

[18] H. Murakami, R. Mizuta, and E. Shindo, "Future changes in tropical cyclone activity projected by multi-physics and multi-SST ensemble experiments using the 60-km-mesh MRI-AGCM," *Climate Dynamics*, vol. 39, no. 9-10, pp. 2569–2584, 2012.

[19] K. S. Mogensen, L. Magnusson, and J.-R. Bidlot, "Tropical cyclone sensitivity to ocean coupling in the ECMWF coupled model," *Journal of Geophysical Research: Oceans*, vol. 122, no. 5, pp. 4392–4412, 2017.

[20] E. Scoccimarro, P. G. Fogli, K. A. Reed, S. Gualdi, S. Masina, and A. Navarra, "Tropical cyclone interaction with the ocean: the role of high-frequency (subdaily) coupled processes," *Journal of Climate*, vol. 30, no. 1, pp. 145–162, 2017.

[21] I.-I. Lin, P. Black, J. F. Price et al., "An ocean coupling potential intensity index for tropical cyclones," *Geophysical Research Letters*, vol. 40, no. 9, pp. 1878–1882, 2013.

[22] E. Scoccimarro, A. Bellucci, A. Storto, S. Gualdi, S. Masina, and A. Navarra, "Remote subsurface ocean temperature as a predictor of Atlantic hurricane activity," *Proceedings of the National Academy of Sciences*, vol. 115, no. 45, pp. 11460–11464, 2018.

[23] J. F. Price, "Upper ocean response to a hurricane," *Journal of Physical Oceanography*, vol. 11, no. 2, pp. 153–175, 1981.

[24] K. A. Emanuel, "Thermodynamic control of hurricane intensity," *Nature*, vol. 401, no. 6754, pp. 665–669, 1999.

[25] M. A. Bender and I. Ginis, "Real-case simulations of hurricane-ocean interaction using A high-resolution coupled model: effects on hurricane intensity," *Monthly Weather Review*, vol. 128, no. 4, pp. 917–946, 2000.

[26] Y.-H. Tseng, S. Jan, and D. E. Dietrich, "Modeled oceanic response and sea surface cooling to Typhoon kai-tak," *Terrestrial, Atmospheric & Oceanic Sciences*, vol. 21, no. 1, 2010.

[27] P. Huang, I.-I. Lin, C. Chou, and R.-H. Huang, "Change in ocean subsurface environment to suppress tropical cyclone intensification under global warming," *Nature Communications*, vol. 6, p. 7188, 2015.

[28] Y.-P. Guo and Z.-M. Tan, "Westward migration of tropical cyclone rapid-intensification over the Northwestern Pacific during short duration El Niño," *Nature Communications*, vol. 9, no. 1, p. 1507, 2018.

[29] I. I. Lin, I. F. Pun, and C. C. Lien, ""Category-6" supertyphoon Haiyan in global warming hiatus: contribution from subsurface ocean warming," *Geophysical Research Letters*, vol. 41, no. 23, pp. 8547–8553, 2014.

[30] T. P. Guilderson and D. P. Schrag, "Abrupt shift in subsurface temperatures in the tropical pacific associated with changes in El Niño," *Science*, vol. 281, no. 5374, pp. 240–243, 1998.

[31] J.-Y. Yu, H.-Y. Kao, T. Lee, and S. T. Kim, "Subsurface ocean temperature indices for central-pacific and eastern-pacific types of El Niño and La Niña events," *Theoretical and Applied Climatology*, vol. 103, no. 3-4, pp. 337–344, 2011.

[32] J.-H. Chu, C. R. Sampson, A. S. Levine, and E. Fukada, *The Joint Typhoon Warning Center Tropical Cyclone Best-Tracks, 1945–2000*, Vol. 16, Joint Typhoon Warning Center, Pearl Harbor, HI, USA, 2002.

[33] K. Emanuel, "Increasing destructiveness of tropical cyclones over the past 30 years," *Nature*, vol. 436, no. 7051, pp. 686–688, 2005.

[34] L. Wu and H. Zhao, "Dynamically derived tropical cyclone intensity changes over the western North Pacific," *Journal of Climate*, vol. 25, no. 1, pp. 89–98, 2012.

[35] M. Ying, W. Zhang, H. Yu et al., "An overview of the China Meteorological Administration tropical cyclone database," *Journal of Atmospheric and Oceanic Technology*, vol. 31, no. 2, pp. 287–301, 2014.

[36] M. Ishii, A. Shouji, S. Sugimoto, and T. Matsumoto, "Objective analyses of sea-surface temperature and marine meteorological variables for the 20th century using ICOADS and the Kobe collection," *International Journal of Climatology*, vol. 25, no. 7, pp. 865–879, 2005.

[37] E. Kalnay, M. Kanamitsu, R. Kistler et al., "The NCEP/NCAR 40-year reanalysis project," *Bulletin of the American Meteorological Society*, vol. 77, no. 3, pp. 437–471, 1996.

[38] N. Rayner, D. E. Parker, E. Horton et al., "Global analyses of sea surface temperature, sea ice, and night marine air temperature since the late nineteenth century," *Journal of Geophysical Research: Atmospheres*, vol. 108, no. D14, 2003.

[39] L. K. Shay, G. J. Goni, and P. G. Black, "Effects of a warm oceanic feature on Hurricane Opal," *Monthly Weather Review*, vol. 128, no. 5, pp. 1366–1383, 2000.

[40] I. D. Lloyd and G. A. Vecchi, "Observational evidence for oceanic controls on hurricane intensity," *Journal of Climate*, vol. 24, no. 4, pp. 1138–1153, 2011.

[41] T. Nitta, "Convective activities in the tropical western Pacific and their impact on the Northern Hemisphere summer circulation," *Journal of the Meteorological Society of Japan. Ser. II*, vol. 65, no. 3, pp. 373–390, 1987.

[42] R. Huang and F. Sun, "Impacts of the tropical western Pacific on the East Asian summer monsoon," *Journal of the Meteorological Society of Japan. Ser. II*, vol. 70, no. 1B, pp. 243–256, 1992.

[43] S. A. Good, M. J. Martin, and N. A. Rayner, "EN4: quality controlled ocean temperature and salinity profiles and monthly objective analyses with uncertainty estimates," *Journal of Geophysical Research: Oceans*, vol. 118, no. 12, pp. 6704–6716, 2013.

[44] Y. Liu and G. Chen, "Intensified influence of the ENSO Modoki on boreal summer tropical cyclone genesis over the western North Pacific since the early 1990s," *International Journal of Climatology*, vol. 38, pp. e1258–e1265, 2018.

[45] Y. Liu, P. Huang, and G. Chen, "Impacts of the combined modes of the tropical Indo-Pacific sea surface temperature anomalies on the tropical cyclone genesis over the western North Pacific," *International Journal of Climatology*, vol. 39, no. 4, pp. 2108–2119, 2019.

[46] G. Chen and C.-Y. Tam, "Different impacts of two kinds of Pacific Ocean warming on tropical cyclone frequency over the western North Pacific," *Geophysical Research Letters*, vol. 37, no. 1, 2010.

[47] S. J. Camargo and A. H. Sobel, "Western North Pacific tropical cyclone intensity and ENSO," *Journal of Climate*, vol. 18, no. 15, pp. 2996–3006, 2005.

[48] K. Emanuel and D. S. Nolan, "Tropical cyclone activity and the global climate system," in *Proceedings of the 26th Conference on Hurricanes and Tropical Meteorolgy*, Miami, FL, USA, May 2004.

[49] K. A. Emanuel, "The maximum intensity of hurricanes," *Journal of the Atmospheric Sciences*, vol. 45, no. 7, pp. 1143–1155, 1988.

[50] K. A. Emanuel, "Sensitivity of tropical cyclones to surface exchange coefficients and a revised steady-state model incorporating eye dynamics," *Journal of the Atmospheric Sciences*, vol. 52, no. 22, pp. 3969–3976, 1995.

[51] K. Emanuel, "A statistical analysis of tropical cyclone intensity," *Monthly Weather Review*, vol. 128, no. 4, pp. 1139–1152, 2000.

[52] M. Zhang, L. Zhou, D. Chen, and C. Wang, "A genesis potential index for Western North Pacific tropical cyclones by using oceanic parameters," *Journal of Geophysical Research: Oceans*, vol. 121, no. 9, pp. 7176–7191, 2016.

[53] R. O. R. Y. Thompson, "Climatological numerical models of the surface mixed layer of the ocean," *Journal of Physical Oceanography*, vol. 6, no. 4, pp. 496–503, 1976.

[54] Z. Li, W. Yu, T. Li, V. S. N. Murty, and F. Tangang, "Bimodal character of cyclone climatology in the bay of bengal modulated by monsoon seasonal cycle," *Journal of Climate*, vol. 26, no. 3, pp. 1033–1046, 2013.